DIPARTIMENTO DI INGEGNERIA DELL'AMBIENTE,

DEL TERRITORIO E DELLE INFRASTRUTTURE

Corso di Laurea Magistrale in

INGEGNERIA PER L'AMBIENTE E IL TERRITORIO

TESI DI LAUREA MAGISTRALE

Contraction Section Design for Inlets in Open Channel Facilities: A Case Study.

A.a. 2023/2024

Relatore:

Prof. Costantino Manes

Candidata:

Zahra Saberian

March 2024

ABSTRACT

This thesis investigates the inlet design for a new open channel facility in the fluid mechanics laboratory of the Polytechnic University of Turin. In the laboratory, we currently have an outdated channel that must be upgraded. This study focuses on the implementation of a contraction section in the upstream to improve the water flow properties in the test section. The study analyzes and numerically simulates flow parameters using ANSYS FLUENT, including uniformity, turbulence intensity and boundary layer separation along the contraction.

The design, which was constrained by the laboratory's maximum channel accessible size of around 4.4 meters wide and a maximum flow rate of 300 litters per second, was created with Solid Works software. The contraction intake and outlet are rectangular, with a free surface resembling a half-wind tunnel. The existing research suggests polynomials of orders (3rd, 5th, and 7th) for contraction curves. In this work, a unique analysis is performed for the 3rd order shaped profile for lateral and vertical contraction with a contraction ratio of 8 and an L/D ratio of 0.89, which will then be connected to the test section, the study of which is outside the scope of this work.

The outcome demonstrated that the recommended contraction design, a 3rd-order wall profile with a length of 1.8 m, is one of the ideal approaches to providing a consistent flow in the outlet without flow separation in both laminar and turbulent flow. It is crucial to keep in mind that not all tunnel types subject themselves to the same ideal design. A number of profiles are re-examined for similar tunnels under various operating circumstances.

Keywords: fluid mechanics, Water channel, ANSYS FLUENT

Contents

List of Figures 4
List of Tables 5
Chapter 1 6
Introduction 6
2 Theoretical Studies 11
2.1 design constrains 11
2.2 contraction curve 12
2.2.2 L/H_i ratio 14
2.2.3 contraction length 14
2.3 contraction design 15
3 computational methods 16
3-1 laminar flow 16
3-1-1 mesh generation: 16
3-1-2 laminar flow rate 17
3-1-3 Mesh independency study 18
3-1-4 CFD model setting: 19
3.2 Turbulent model: 20
3-2-1 Turbulent flow mesh generation 21
3-2-2 CFD model setting in turbulent flow 23
3 Numerical result and discussion 25
3-1 laminar Flow result 25
3-2: turbulent result 28
5 Conclusion 31
References 32

List of Figures

Figure 1: third order contraction shape. 14
Figure 2:contraction design. 15
Figure 3: cad model of contraction. 16
Figure 4:sample of model meshing 17
Figure 5:residual convergence plot for laminar study 20
Figure 6: y+ distribution in wall in 5mm mesh size 22
Figure 7: residual convergence plot for turbulent flow 24
Figure 8: velocity contour in outlet in 0.3 L/s laminar flow 25
Figure 9: streamline for laminar flow 26
Figure 10: velocity contour of laminar flow in 1.4L/s 27
Figure 11:streamline and pressure distribution in laminar flow 27
Figure 12: velocity distribution in the outlet in 300L/s for turbulent flow 28
Figure 13:turbulent kinetic energy distribution in 300L/s 29
Figure 14: turbulent kinetic energy distribution 29
Figure 15:skin friction coefficient 30

List of Tables

Table 1:Boundary conditions for solving the 5th order polynomial. 12
Table 2: adapting polynomial shapes for contraction. 13
Table 3: mesh independence study of laminar flow 19
Table 4: mesh study of turbulent flow 22
Table 5:uniformity index in laminar flow.....28
Table 6: numerical result of turbulent flow 30

Chapter 1

Introduction

Starting experimental research in hydraulic engineering and fluid dynamics demands the development of laboratory channels, a fundamental step with scientific significance. These channels are essential platforms for studying hydraulic structures, sediment transport phenomena, and fluid flow dynamics. At their core, these channels represent not only conduits of water, but also conduits of knowledge, providing researchers with a controlled setting to study all aspects of hydraulic behaviour. In these channels, maintaining flow homogeneity and exercising strict control are necessary for the quest of scientific rigor. Hydraulic conditions in these channels have a significant impact on the accuracy and integrity of experimental results. Hydraulic conditions need to be carefully managed in the same way as scientists calibrate their equipment to guarantee the accuracy and repeatability of the data obtained from experiments. The achievement of exact control and uniform flow within these lab channels is, in essence, the key to the scientific validity of hydraulic investigations.

A fundamental component of experimental fluid dynamics, contracture nozzles are positioned upstream of water channels meant for in-depth flow investigations. These nozzles are multifunctional in that they use science to precisely and elegantly control the channel's flow dynamics. At first, the flow velocity is accelerated by the constriction that these nozzles cause. This increased speed not only makes it easier to place support structures like screens and honeycomb patterns in areas where flow is slower, but it also saves a significant amount of energy by reducing pressure losses all the way through the tunnel. (Mehta J. H., 1988)

Furthermore, these contractions influence the fundamental principles of flow dynamics, balancing the flow field by reducing variances in mean and fluctuation velocities at various cross-sections. These nozzles ensure complete pressure is maintained throughout the contraction process, which promotes a regime of greater uniformity and an environment that is

ideal for accurate testing. Reductions in velocity fluctuations have the cascading effect of reducing the need for screens in the settling chamber, which further reduces pressure losses and maximizes the effectiveness of the experimental setup. (Mehta J. H., 1988)

The contraction ratio is a critical factor that has been thoroughly studied and determined throughout time by scientists to be essential to the effectiveness of contracture nozzles. Many research that have been published in the annals of fluid dynamics literature have carefully examined parameters that range from wall shape to the choice of the ideal contraction ratio, resulting in a body of knowledge that guides the design and performance measurement of these crucial elements. To eliminate flow separation and create a smooth, unwavering stream, the overall goal of designing a contraction section is to create a symphony of the flow.These considerations lead to the conclusion that the optimal contraction length is a trade-off between efficiency and practicality, with the goal of minimizing boundary layer thickness at the exit plane while meeting strict non-uniformity. (Su, 1991)

Following these guidelines, the optimal contraction length is determined by striking a compromise between practicality and effectiveness, with the goal of minimizing boundary layer thickness at the exit plane while meeting strict non-uniformity requirements (usually 0.5% outside the boundary layer). Large contraction ratios improve performance, but they also have drawbacks. Particularly, they may cause problems like noise and separation at the end of the tunnel, which would be made worse by higher construction and maintenance expenses. A consensus based on empirical evidence from the operation of small, low-speed wind tunnels with cross-sectional areas of less than 0.5 m2 and free-stream velocities below 40 m/s has determined optimal contraction ratios are generally between 6 and 10. (Mehta J. H., 1988)

Apart from the crucial evaluation of the contraction ratio, another essential factor in the design of laboratory channels is the selection of the cross-sectional form. The subtleties of fluid dynamics reveal a complex relationship between geometry and flow behavior, which is especially clear when considering corner flows inside contractions. Due to the lower velocities that these areas are known for, the tendency for separation is stronger here. In addition, the convergence of secondary flows and crossflows in the vicinity of the corners emphasizes how critical it is to carefully design the cross-sectional form in order to promote ideal flow conditions. (Bradshaw, November 1979)

Cross-sectional shape compatibility with other tunnel components, particularly the test section, is important. This has been highlighted by recent developments in fluid dynamics research. It is an unexpected find that, when separation is not present, corner flow characteristics typically stay localized and have little effect on the overall flow dynamics along the test wall throughout the majority of the span. Thus, the choice of cross-sectional shape becomes a fine trade-off between reducing the impacts of separation and making sure that the tunnel's overall design is compatible. (Fang, 1997)

The design process revolves around determining the length and shape of the contraction wall, which is driven by knowledge gained from a thorough examination of the study on contraction design. To improve the efficiency of 2D channel designs, suggestions are in favor of using polynomial forms, specifically the 3rd, 5th, and 7th orders. By means of a methodical investigation of diverse contraction profiles, guided by the previously defined parameters, scientists endeavor to clarify the complex relationship between geometry and flow dynamics. This, in turn, improves the design of laboratory channels to open up new avenues for hydraulic engineering and fluid dynamics experimentation. (Mehta J. H., 1988)

At the esteemed Polytechnic University of Turin, an original case study serves as a foundation for innovation and scientific inquiry in the effort of advancing fluid mechanics research. This

thesis explores the complexity of a contraction zone inlet with a third order polynomial shape in an open water channel through a thorough analytical and numerical analysis. This work, with its L/D ratio of 0.89, contraction rate of 8, and rectangular shape that serves as both an inlet and an outlet, creates precedent in hydraulic engineering and fluid dynamics.

Fundamentally, this project's main goal is to carefully examine the flow characteristics that are embedded in the planned water channel. By means of an integrated strategy that includes both computational fluid dynamics (CFD) simulations and analytical modeling, the study aims to reveal important features that support the fluid dynamics environment. The wall pressure distributions are the most important of these since they provide important information about the forces that the fluid in motion exerts on the channel walls. It also explores the complex interaction of streamline patterns, providing a pictorial representation of the paths that the liquid particles take through the channel.

Identifying flow separation events is essential to the study's scope since it is a phenomenon that has significant effects on the effectiveness and dependability of hydraulic tests. Through an analysis of the relationship between flow rates and geometric arrangements, the study seeks to identify the mechanisms that control separation and open the door to improved design approaches that minimize its negative effects.In addition, the research aims to clarify the velocity profiles that flow through the channel in order to provide a more detailed picture of the fluid dynamics environment. By carefully examining and interpreting these profiles, scientists hope to uncover hidden trends and irregularities that will contribute to our understanding of fluid behavior in the setting of lab channels.

Underlining the fact that tunnel design is complex and that there isn't a single optimum configuration that works greatest in every situation is essential. For this reason, the study takes a comprehensive approach, revisiting multiple profiles in a range of settings, therefore guaranteeing a thorough and solid investigation of the design space. Fluid mechanics research

at the Polytechnic University of Turin is seeking to achieve new heights of excellence and innovation by optimizing the contraction wall profile and length. Through analytical and numerical inquiry, this can be done in order to improve the performance of the contraction section.

2 Theoretical Studies

2.1 design constrains

During the laborious design of the contraction zone for the laboratory channel at the Polytechnic University of Turin, several significant constraints were closely considered in order to ensure optimal performance and compliance with experimental requirements.

Firstly, the maximum width less than 4.5 meters that could be allocated to the new laboratory channel served as the boundary for the inlet cross-section. This parameter is fundamental in design; it determines the channel's overall dimensions and establishes the framework for further design considerations.

Furthermore, the inlet and outlet heights (Hi and Ho) of the channel were specified to correspond with the expected water depths needed for experimental purposes. In this instance, the operational requirements and pragmatic considerations of experimental setups within the laboratory setting were reflected in the assumption of a water depth of roughly 2 meters at the input and 0.5 meters at the outflow.

Moreover, the inlet's maximum flow rate was limited to less than 300 liters per second, which is an important boundary condition for turbulent flow regimes. This restriction serves to both guarantee the stability and safety of the experimental setup and emphasize how crucial it is to keep the flow conditions in the channel under control and manageable.

Through strict adherence to these limitations, the contraction zone's design is customized to fulfill the unique operational needs and experimental goals of the laboratory channel. The resulting design promises to give strong and dependable performance through a careful synthesis of scientific rigor and engineering principles, allowing innovative fluid dynamics research at the Polytechnic University of Turin.

2.2 contraction curve

The contraction curve equation provided represents an advanced mathematical model designed to describe the complexity of the flow behavior in the lab channel. The 5th order equation takes on the following form when it is expressed in terms of the normalized distance downstream ($\xi = x/L$), where L is the contraction length (Mehta J. H., 1988):

$$Y = a\xi^5 + b\xi^4 + c\xi^3 + d\xi^2 + e\xi + f \qquad 2\text{-}1$$

Each of the following coefficients(a,b,c,d,e,f) has a unique function in forming the contraction curve and adding to the complex interaction of flow dynamics in the channel. The more complex variables capture each aspect of the contraction profile, indicating small changes and departures from the idealized flow behaviour. The coefficient for 5th order polynomial contraction profile can be obtained utilizing the following boundary condition in table 1, we can get the coefficients a, b, c, d, e, and f.

***Table 1**:Boundary conditions for solving the 5th order polynomial.*

At the inlet	At the turning point	At the exit
$Y(0) = H_i$	$\frac{d^2}{dx^2}y = 0$	$Y(l) = H_e$
$\frac{d}{dx}Y(0) = 0$		$\frac{d}{dx}Y(l) = 0$
$\frac{d^2}{dx^2}y(0) = 0$		$\frac{d^2}{dx^2}y(l) = 0$

It is demonstrated that terms f, e, and d are zero. Consequently, the following equations can be found:

- a +b +c =1
- 5a +4b +3c =0
- 20a +12b +6c = 0

Solving and setting a, b, and c to 6, -15, and 10 yields:

$$Y = Hi - (Hi - He)\,[6\,(x/l)5 - 15(x/l)4 + 10(x/l)3] \qquad 2\text{-}2$$

Through the same procedure, we can obtain the following contraction curve profile suggestion.

***Table 2**: adapting polynomial shapes for contraction.*

Third order polynomial	$Y = H_i - (H_i - H_e)[-2\xi^3 + 3\xi^2]$
Fifth Order Polynomial	$Y = Hi - (Hi - He)\,[6\,(\xi)5 - 15(\xi)4 + 10(\xi)3]$
Seventh Order Polynomial	$Y = Hi - (Hi - He)[-20(\xi)7 + 70(\xi)6 - 84(\xi)5 + 35(\xi)4]$

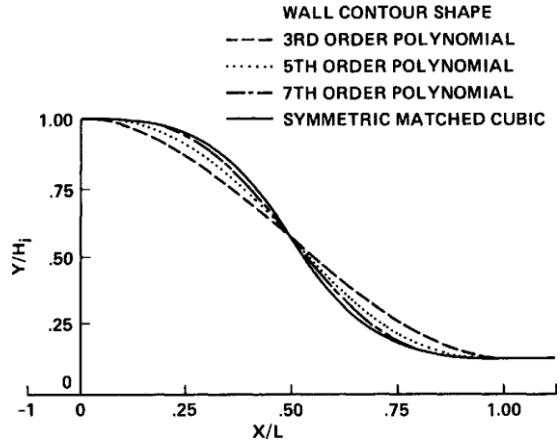

***Figure1:** Wall contour shapes of contractions tested. (Mehta J. H., 1988)*

In Table 2 (ξ=x/L) is the normalized distance downstream for third order polynomial can be employed directly by indicating the necessary contraction length as discussed above. Here, L

represents the contraction length, while Hi and Ho are the contraction inlet and exit water depth, respectively.

Figure 2 shows the form of third order contraction shape . The inflection point is in the middle, and the contraction's inlet and outflow have 0 slopes.

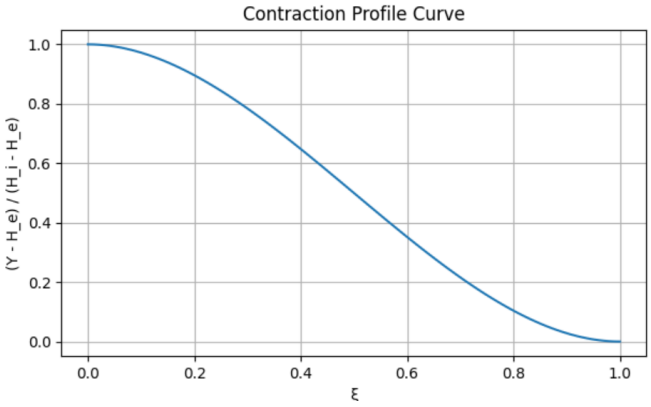

Figure 1: *third order contraction shape.*

2.2.2 L/H_i ratio

For Length/Height (L/Hi) ratios greater than 1.79 and less than 0.667, separation happens for rectangular contractions with a fifth order and third-order polynomial form [2]. For our contraction, we may anticipate that these numbers will be similar. Conversely, considering the estimated useful length, L/Hi ratios greater than 1.5 would necessitate a shorter test section and/or a tighter distance between the contraction and the honeycomb. According to the studies, a minimum acceptable L/H for our criteria was 0.89. (Bradshaw, November 1979)

2.2.3 contraction length

Maintaining a short nozzle length is crucial in hydraulic engineering to minimize pressure losses and overall channel length. This principle aligns with Bernoulli's equation, which states that the sum of kinetic, potential, and pressure energies along a streamline remains constant. By reducing the length-to-diameter (L/D) ratio to approximately 0.89, the nozzle achieves an optimal balance between minimizing pressure losses and ensuring efficient fluid flow.

At this L/D ratio, the contraction length, representing the section where the fluid converges to pass through the nozzle, is approximately 1.8 meters. This contraction length is determined based on fluid dynamics principles, considering factors such as Reynolds number, viscosity, and flow velocity.

2.3 contraction design

The fluid dynamics of the system are further complicated by adding the concept of a contraction zone, where the surface meets air, like a half wind tunnel. The boundary conditions and flow characteristics are impacted by the interaction between the contraction zone's surface and the air, especially regarding surface roughness and slip circumstances.

In fluid dynamics, several variables, including viscosity, surface roughness, and slip conditions, can typically affect how fluids behave near solid surfaces. The relative motion between a fluid and a solid surface is referred to as slip, and it may occur for a variety of reasons, including hydrodynamic slippage or molecular slide.

If the contraction zone's surface stays level from the inlet to the outflow, there will likely be a gradual shift in geometry rather than any sharp alterations. To minimize pressure losses and maximize flow efficiency, this design promotes laminar flow conditions and lowers turbulence.

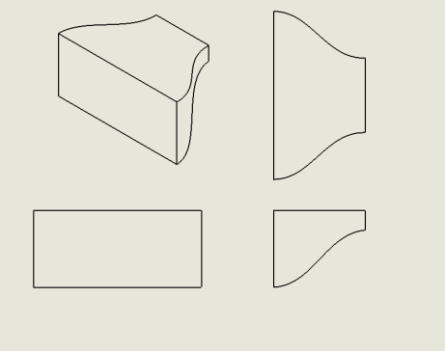

Figure 2:*contraction design.*

3 computational methods

Solidworks [2022] was used to create CAD model for numerical simulations of the contraction. This model was imported into Ansys Fluent, where it was meshed and numerically simulated. Water flow in this study was considered to be adiabatic, steady-state, and incompressible. Simulations were performed in both laminar and turbulent flow.

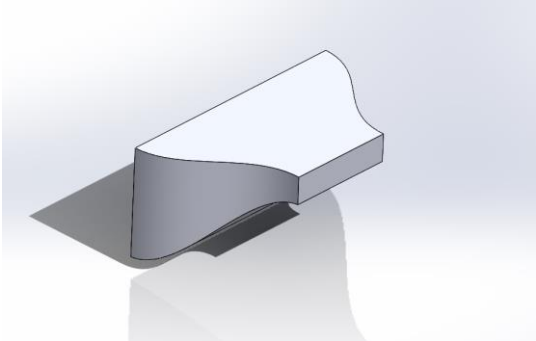

***Figure 3**: cad model of contraction.*

To minimize simulation time while ensuring accurate results, it was decided to exploit the symmetry of the contraction with respect to the x-axis. Consequently, the simulation was carried out on a 1/2 scaled version of the initial design.

3-1 laminar flow

3-1-1 mesh generation:

A careful process was used to create a mesh that could faithfully represent the complex flow phenomena while preserving computational efficiency in order to simulate laminar flow inside the laboratory channel. By utilizing a tetrahedral mesh type and the patch conforming approach, the mesh quality and accuracy to the physical geometry were optimized. Given the importance of boundary layer effects in laminar flow simulations, the mesh close to the walls was given special consideration. To achieve this, a growth rate of 1.2 in conjunction with a maximum inflation layer thickness of 10-15 layers was used. This tactical decision made it easier to create

a mesh that was denser along the walls' edges, which allowed boundary layer phenomena to be represented more accurately (Wachem, 2011).

A strict evaluation of the mesh's quality was conducted utilizing criteria like average and maximum skewness. The maximum skewness was limited to 0.75 and the average skewness was carefully regulated at 0.22 to preserve high-quality meshing. These strict requirements made sure that a well-organized mesh with little distortion was produced, which established a strong basis for precise and trustworthy laminar flow simulations inside the lab channel. Below is a sample of the final meshing result for the computational domain:

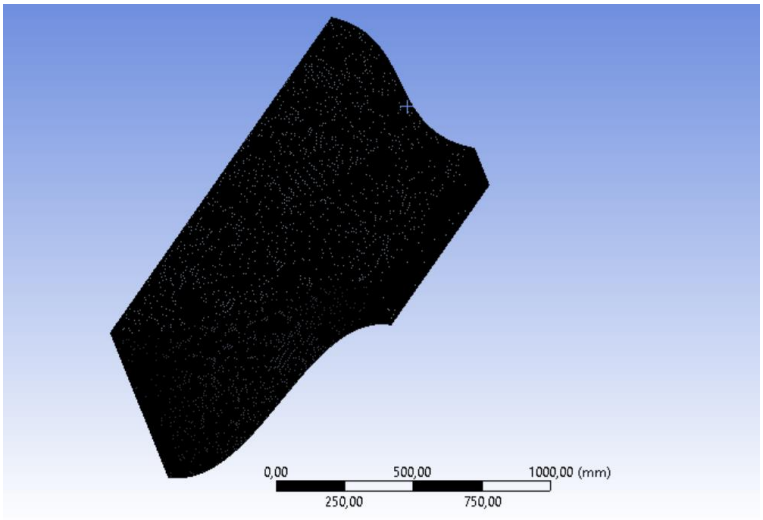

***Figure** 4:sample of model meshing*

3-1-2 laminar flow rate

In the early phases of design, when careful planning and forethought are critical, a fundamental standard was set to guarantee laminar flow in the lab channel. This standard, which has its origins in the basic ideas of fluid dynamics, is represented by an outlet condition Reynolds number threshold of less than 400. By setting this cutoff point, we can assure that laminar flow

will occur throughout our contraction zone. A guiding light that illuminates the expected domain of flow behaviour in our system is the Reynolds number, a dimensionless parameter that captures the balance between inertial and viscous forces within a fluid flow. We provide researchers with the assurance of predictable and well-characterized fluid behavior with a Reynolds number below 400 at the outlet condition, so fostering trust in the laminar nature of the flow (White, 1994). By taking this calculated risk, we are able to protect the integrity of our experimental setup and set the stage for accurate and insightful investigations of laminar flow events in the laboratory channel.

Utilizing the prescribed formula $U_{avg}=\frac{400\nu}{H}$, where ν represents the kinematic viscosity and H signifies the height of water in the outlet plate after scaling (equivalent to 0.19 meters), we calculate the average velocity *U*avg to be 2.1 e-3m/s.

Subsequently, the mass flow rate (Q) is determined by multiplying the average velocity () by the cross-sectional area (A) of the outlet. Based on these calculations, the mass flow rate is found to be 0.3 L/s.

3-1-3 Mesh independency study

Results from simulations cannot be considered reliable until it is proven that differences in flow characteristics are caused by changing conditions rather than the number and type of grid cells (mesh independence). To ensure grid viability, a novel investigation was conducted to determine the precise number of cells required for a reliable study. This inquiry involved monitoring changes to specific flow parameters until they stabilized or the amount of change was minimized. For each velocity, five simulations were performed, resulting in a total of twenty simulations for laminar and turbulent flow combined. The results demonstrate a sufficient level of independence of certain flow field properties from variations in mesh size

Table 3: mesh independence study of laminar flow

Element size(mm)	Numbers of elements	Exit averaged velocity (m/s)	Reynolds Numbers	Exit Total pressure (Pa)
20	24327	0.002153585	409.18	0.002534465
15	55440	0.00215459	409.37	0.002534439
10	178080	0.0021558	409.60	0.002534321
6	836352	0.00215742	409.91	0.0025343
3	6652800	0.002157435	409.91	0.00253429

3-1-4 CFD model setting:

The domain zones included an inlet plane, an exit plane, 2 wall, one symmetry plane, and a free surface. A pressure-based solver using absolute velocity formulation was chosen. The velocity was set for the inlet with zero initial gauge pressure and the boundary condition for outlet was the pressure. The no-slip criterion was applied to the walls. The zero-shear stress was set for free surface.

Convergence of the solution was deemed adequate when the velocity and continuity residuals fell below (1e-4) and (1e-6), respectively. The convergence of these residuals was monitored throughout the simulation to ensure accuracy and reliability. (Figure6) is a sample curve illustrating the convergence of residuals for a laminar flow scenario.

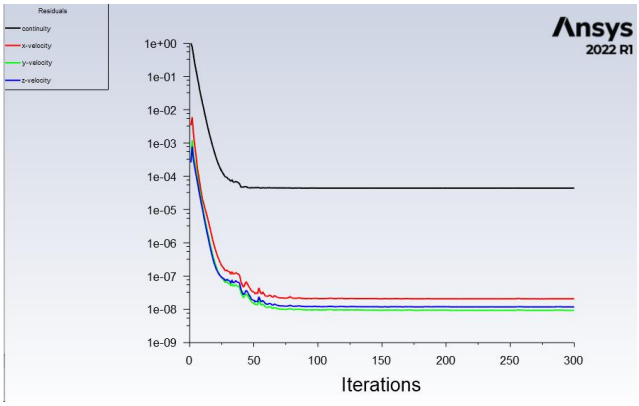

***Figure 5**:residual convergence plot for laminar study*

3.2 Turbulent model:

The k-epsilon standard wall function turbulence model with double precision was used in the series of simulations. Two transport equations are used in this model: one for turbulent dissipation rate (ε) and another for turbulent kinetic energy (k). These equations, which are derived from the Reynolds-averaged Navier-Stokes equations (RANS), include closure terms to fully capture the impact of turbulence on the mean flow field.

The k-epsilon standard wall function model is commonly used in Computational Fluid Dynamics (CFD) simulations due to its effectiveness in describing turbulent boundary layers that are close to solid surfaces. By assuming a logarithmic velocity profile and using empirical relationships to predict velocity and turbulence at the first grid point away from the wall, this model approximates the behavior of near-wall flow. This method eliminates the need for highly precise mesh resolution along the wall, enabling computationally efficient simulations.

3-2-1 Turbulent flow mesh generation

first grid point adjacent to the wall in this step requires careful consideration, as it must lie within the logarithmic region to satisfy the condition for standard wall function usage near the walls. To maximize the number of grid points in the boundary layer, the first grid point should ideally be positioned as close to the lower boundary of the logarithmic region as possible, typically within the range of 30 < y+ < 100 in dimensionless distance. Since there's no necessity to fully resolve the near-wall region affected by viscosity, employing the wall-function approach conserves a significant number of computational resources.

The calculation of the dimensionless wall distance (y+) was performed according to the equation1 .

$$Y^{+} = \frac{yu*}{\nu} \qquad 3\text{-}1$$

where y is the distance from the wall, $u*$ is the friction velocity, and ν is the kinematic viscosity.

$$u* = \frac{\tau_w}{\rho} \qquad 3\text{-}2$$

τ_{w} that is wall shear stress is obtained from

$$\tau_w = \rho\nu \left.\frac{d\langle U\rangle}{dy}\right|_{y=0} \qquad 3\text{-}3$$

The initial estimation of the mesh size near the wall was theoretically calculatedto achieve a target Y+ value of approximately 5 mm based on average velocity . This estimation was crucial for ensuring proper resolution of the near-wall region in the computational domain. To validate the accuracy of this estimation, the simulation results were compared with those obtained from ANSYS Fluent, a widely used computational fluid dynamics (CFD) software.

After confirming the correctness of the initial mesh size estimation through comparison with ANSYS Fluent results, the simulation was repeated with various mesh sizes. This iterative process allowed for a comprehensive study of the simulation accuracy under different mesh resolutions. By systematically varying the mesh size and analyzing the resulting simulation outcomes, insights into the impact of mesh resolution on the accuracy of the simulation were gained.

This approach not only validated the initial mesh size estimation but also provided valuable information regarding the sensitivity of the simulation results to changes in mesh resolution. Ultimately, this iterative process helped ensure the reliability and accuracy of the CFD simulations conducted for the study.

***Table 4**: mesh study of turbulent flow*

Element size(mm)	Number of elements	Averaged Exit velocity (m/S)	Turbulent intensity(%)	Exit total pressure(Pa)	Averaged kinetic energy($m^2.s^{-2}$)
15	464156	0.542762	8.1244	152.6183	0.01021
10	1275976	0.54277	8.124062	152.6178	0.0102198
7	1455843	0.5427679	8.124069	152.6164	0.01023003
5	5048832	0.5429315	8.433896	151.5585	0.01087196

For each simulation iteration, the y+ value was computed to assess compliance with the requirements for the wall standard wall function. An example of this analysis for a 5 mm mesh size is depicted in the figure below.

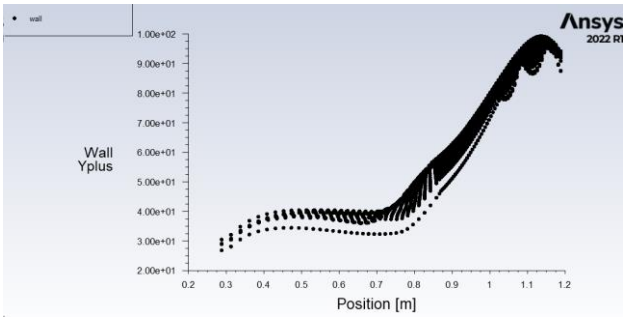

***Figure 6:** y+ distribution in wall in 5mm mesh size*

3-2-2 CFD model setting in turbulent flow

The simulation boundary conditions were configured as follows: velocity was prescribed at the inlet, while pressure was specified at the outlet. Additionally, a symmetry plane condition was applied. The no-slip condition was enforced for walls, and zero shear stress was set for free surfaces, mirroring the conditions utilized in the laminar flow simulations.

Pressure-velocity coupling was achieved using the Semi-Implicit Method for Pressure Linked Equation (SIMPLE) approach, resulting in separate equations for pressure and velocity. Spatial discretization was based on a least squares cell gradient. The remaining equations, including pressure, momentum, turbulent kinetic energy, and specific dissipation rate, were discretized using the second-order upwind method.

Standard initialization was performed using data derived from the inlet. Under relaxation factors were adjusted to 0.5 for pressure, 0.5 for momentum, and 0.75 for turbulent kinetic energy and specific dissipation rate to optimize convergence.

Convergence criteria were set at 1e-6 for velocities and 1e-3 for other variables such as turbulent kinetic energy, dissipation rate, and continuity. Figure 8 illustrates an example of a residual plot for turbulent flow simulation. To establish the boundary condition at the inlet, turbulent parameters including turbulent kinetic energy (equation 2.1) (Batchelor, 2000)and turbulent dissipation rate (equation 2.2) were defined in accordance with the criteria specified by the turbulence model .

$$K = \frac{3}{2}\left(\langle u'^2 \rangle + \langle v'^2 \rangle + \langle w'^2 \rangle \right) \qquad 2.1$$

in which u′,v′,w′ represent the fluctuations of velocity components in the x,y,z directions, respectively .the turbulent dissipation rate will obtain from the equation2.2.

$$\varepsilon = C_{\mu}^{3/4} \frac{K^{\frac{3}{2}}}{L} \qquad 2.2$$

In which C_{μ} is universal and constant and equal to 0.09. (Wachem, 2011)

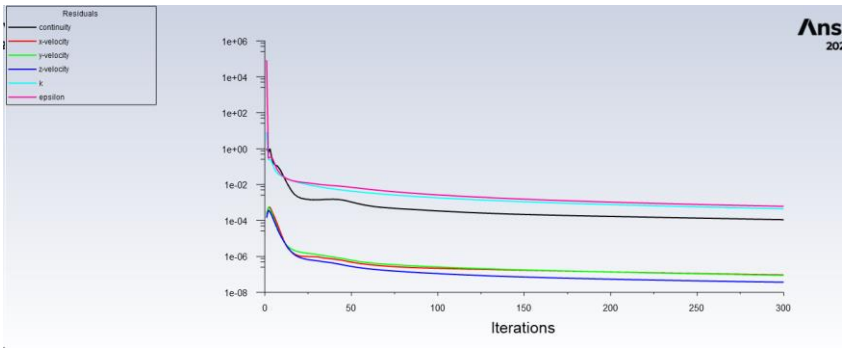

Figure 7: *residual convergence plot for turbulent flow*

3 Numerical result and discussion

The numerical analysis encompasses simulations of the model with varying mass flow rates, specifically 1.4 L/s and 0.3 L/s for laminar flow, and 150 L/s and 300 L/s for turbulent flow. Flow uniformity assessments are conducted by analyzing the velocity distribution at the exit plane, as depicted in Figure 3. Additionally, streamline visualizations are utilized to compare the contraction behavior between laminar and turbulent flows.

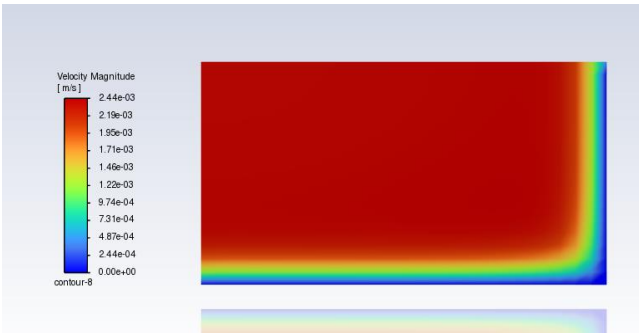

Figure 8: *velocity contour in outlet in 0.3 L/s laminar flow*

3-1 laminar Flow result

Sufficient uniformity at the outlet is demonstrated by the velocity contours(figure 9). When it advances away from the contraction wall, the velocity increases uniformly as expected. Our expectations are supported by this observation, which shows a steady flow behavior at the outflow. For the experimental setup to provide consistent and precise fluid flow parameters, there must be a uniformity in the velocity distribution away from the contraction zone wall.

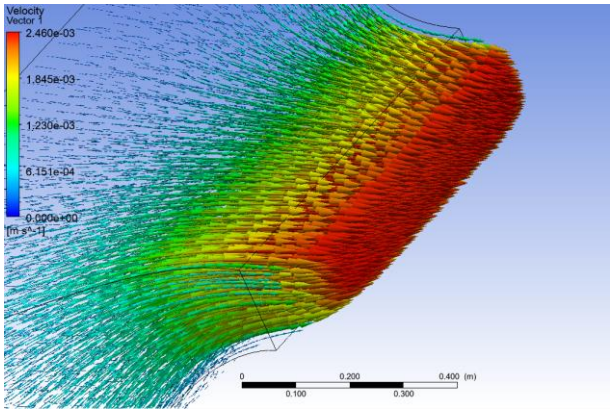

***Figure 9**: streamline for laminar flow*

The streamline contour obtained from numerical simulations in ANSYS Fluent did not reveal any instances of reverse flow or separation occurring at the outlet (Figure 10). This observation suggests that the flow remained attached and continuous throughout the simulation domain, without any significant disruptions or recirculation zones developing near the outlet. This absence of reverse flow and separation is indicative of favourable flow conditions and suggests that the design and operational parameters of the system are conducive to maintaining smooth and efficient fluid dynamics within the experimental setup.

The simulation was repeated with an increased mass flow rate of 1.4 l/s, yet the flow behavior remained consistent with the previous simulation results. Despite the higher mass flow rate, the overall characteristics and patterns of the flow, as observed through various parameters such as velocity profiles, pressure distributions, and streamline patterns, did not exhibit significant changes.(Figure 11)

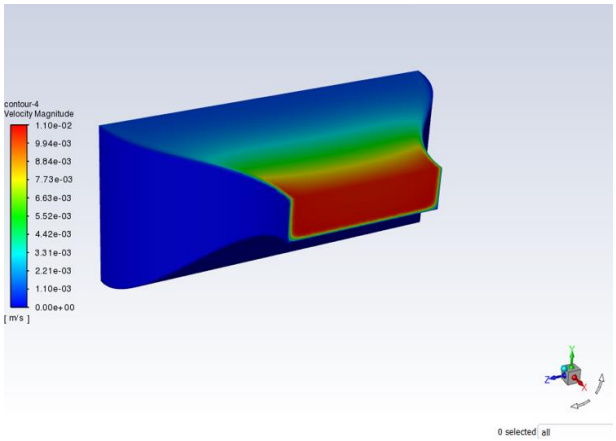

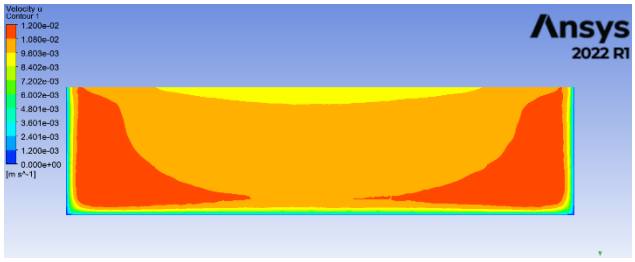

Figure 10: *velocity contour of laminar flow in 1.4L/s*

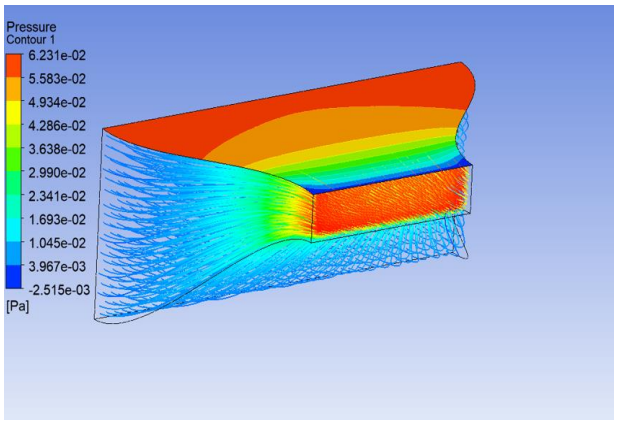

Figure 11:*streamline and pressure distribution in laminar flow*

The uniformity index mass weighted obtained directly was from the Ansys fluent and was shown in the table below :

Table 5:uniformity index in laminar flow

Flow rate(L/s)	Exit velocity ($\bar{u}$)(m/s)	($\bar{u}/u_{max}$)	Uniformity index-mass weighted
0.3	0.00215742	0.976	0.98765
1.4	0.0134651	0.921	0.97651

3-2: turbulent result

The figure below shows the streamline and velocity distribution for mass flow rate 300L/s for the turbulent flow rate :

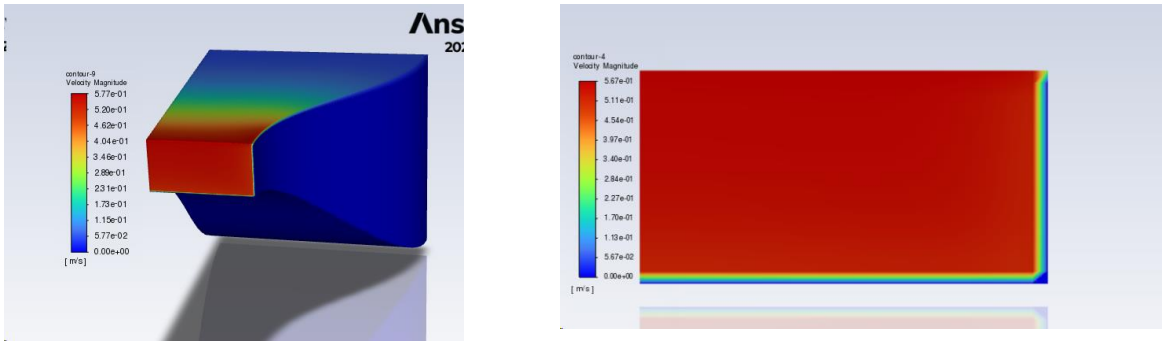

Figure 12: velocity distribution in the outlet in 300L/s for turbulent flow

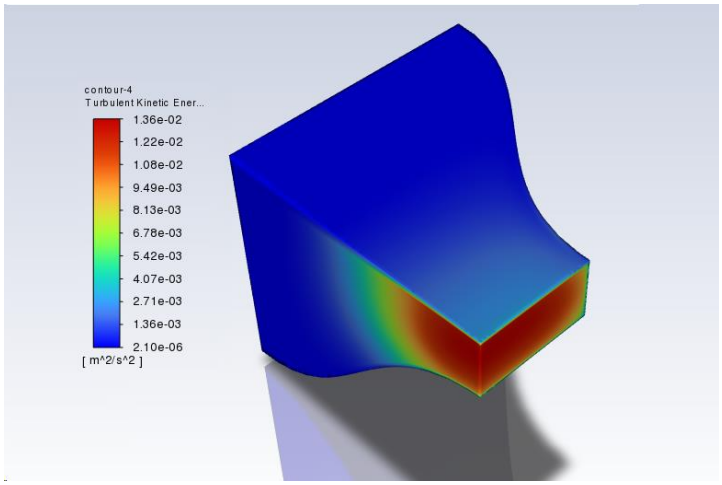

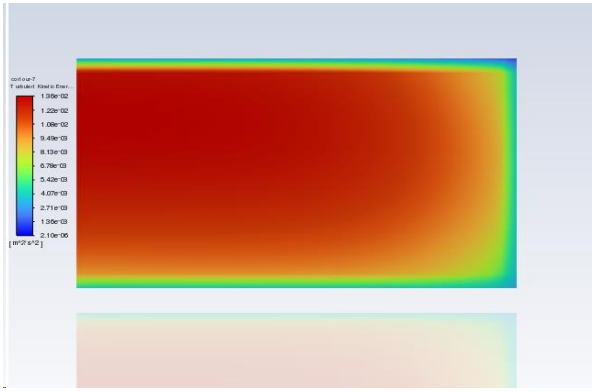

***Figure 13**:turbulent kinetic energy distribution in 300L/s*

The investigation also extended to the examination of turbulent intensity at the exit plane of the contractions. Turbulent intensity was quantified using Equation below, where K represents the turbulent kinetic energy obtained from the numerical analysis, and U denotes the exit velocity, as illustrated in Figure 8.

$$I = \sqrt{\frac{2K}{3u^2}} \qquad 3\text{-}1$$

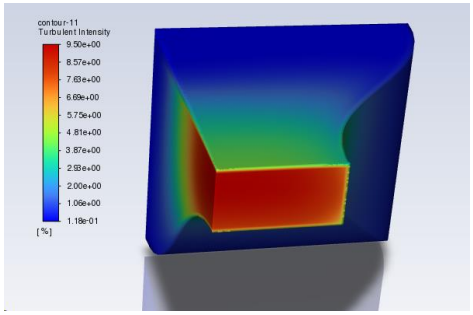

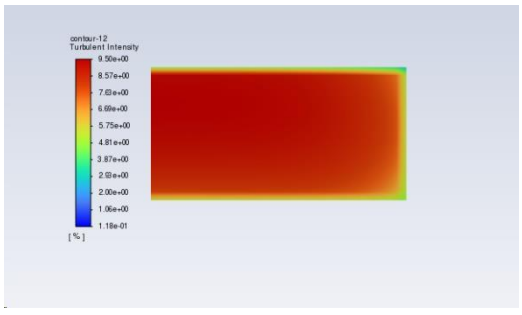

***Figure 14:** turbulent kinetic energy distribution*

Table 3 shows the simulation result for two different flow rate:

Table 6: numerical result of turbulent flow

Flow rate(L/s)	Exit velocity ($\bar{u}$)	Turbulent intensity	Uniformity index-mass weighted	Averged kinetic energy(m^2s^{-2})
300	0.5429315	8.124069	0.9858305	0.01023003
150	0.2455697	2.488149	0.97651	0.001592325

Finally, as illustrated in Figure 9, the simulation results for the skin friction coefficient indicate the absence of zero regions along the contraction walls, indicating no boundary layer separation within the contraction zone.

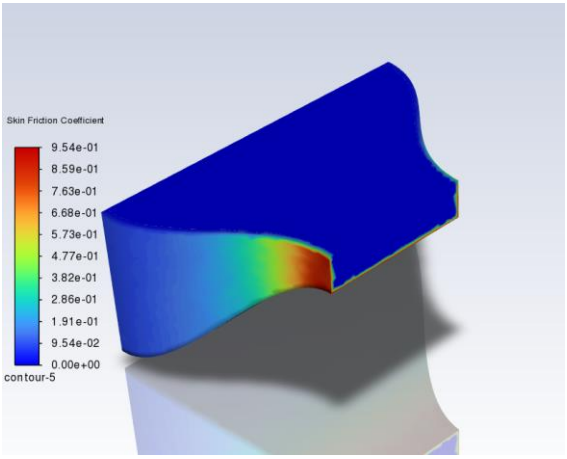

Figure 15:skin friction coefficient

5 Conclusion

This thesis concludes by discussing the important inlet design for a new open channel facility located in the Polytechnic University of Turin's Fluid Mechanics Laboratory. Modernizing the out-of-date channel requires adding a contraction section upstream to improve the test section's water flow characteristics. ANSYS FLUENT numerical simulations and a thorough analysis were used to examine important flow parameters along the contraction, including boundary layer separation, turbulence intensity, and uniformity

Solid Works software was used during the design process, which was limited by the laboratory's requirements of a maximum channel width of roughly 4.4 meters and a maximum flow rate of 300 liters per second. The contraction that resulted had rectangular intake and exit geometries that resembled a half-wind tunnel. Polynomial profiles of orders three, five, and seven were taken into consideration for the contraction curves based on previously conducted research. The analysis of the 3rd-order profile, which has an L/D ratio of 0.89 and a contraction ratio of 8, for lateral and vertical contraction, was the study's singular focus.

The results emphasized that the contraction design that was suggested, which has a 1.8-meter-long, third-order wall profile, was the best method for attaining steady flow in the outlet without encountering flow separation in both laminar and turbulent circumstances. It is important to recognize that different tunnel types and operating conditions may require different designs to be optimal. As a result, additional research ought to be carried out to assess various profiles customized for comparable tunnels and varied operational situations.

Overall, this study presents a case study model for the design and optimization of inlet designs for open channel facilities, leading the way for future research into enhancing flow efficiency and performance in experimental setups.

References

Batchelor, G. K. (2000). *An Introduction to Fluid Dynamics.* Cambridge University Press.

Bradshaw, R. D. (November 1979). *Design Rules for Small Low-Speed Wind Tunnels* . (Aeronautical Journal) pp 718 .

Fang, F. (1997). *A Design Method for Contractions with Square End Sections* . (ASME J. Fluids Eng.) vol 119 .

Ferchichi, D. B. (2005). *Transformation of A Polynomial for A Contraction Wall* . (Journal of Fluids Engineering) vol 127 .

Mehta, J. H. (1988). *Three-Dimensional Wind Tunnel Contractions* . (AIAA JOURNAL) vol 29 .

R, S. J. (2004). *Design and Calibration of a Wind Tunnel with a* . (Proceedings of the 15th Australasian Fluid Mechanics .

Su, Y.-x. (1991). *Flow Analysis and Design of Three-Dimensional Wind Tunnel Contractions.* (AIAA JOURNAL) vol 29 .

Wachem, B. A.-R.-L.-M.-R.-B. (2011). *computational fluid dynamics for Engineers.* Cambridge University Press.

White, F. M. (1994). *Fluid Mechanics 7th ed.*